Kinematics of the young stellar objects associated with the cometary globules in the Gum Nebula

Rumpa Choudhury[1,2]★ and H. C. Bhatt[1]

[1]*Indian Institute of Astrophysics, Bangalore 560034, India*
[2]*University of Calicut, Calicut 673 635, India*

ABSTRACT

An analysis of the proper motion measurements of the young stellar objects (YSOs) associated with the cometary globules (CGs) in the Gum Nebula is presented. While earlier studies based on the radial-velocity measurements of the CGs suggested expansion of the system of the CGs, the observed proper motion of the YSOs shows no evidence for expansion. In particular, the kinematics of two YSOs embedded in CGs are inconsistent with the supernova explosion of the companion of ζ Pup, about 1.5 Myr ago being the cause of the expansion of the system of the CGs. YSOs associated with the CGs share the average proper motion of the member stars of the Vela OB2 association. A few YSOs that have relatively large proper motions are found to show relatively low infrared excesses.

Key words: stars: pre-main-sequence, kinematics – ISM: globules, clouds and H II regions: individual: Gum nebula.

1 INTRODUCTION

The Gum Nebula, a prominent H II region of southern Milky Way, was discovered by Gum (1952). The whole nebula is around $36°$ in diameter (Chanot & Sivan 1983). The true nature of the Gum Nebula is not very clear. Along with the two O-type stars, ζ Pup and γ^2 Velorum, two OB associations, Vela OB2 and Tr 10, have been found in the Gum Nebula region. There are also two supernova remnants (SNRs) in the direction of the Gum Nebula, Pup A and Vela SNR. However, Sridharan (1992) argued that the spatial coincidence of these two SNRs with the Gum Nebula is due to chance superposition. Chanot & Sivan (1983) described the Gum Nebula as an intermediate structure between classical H II region and typical SNR.

About 30 cometary globules (CGs) have been found in the Gum Nebula and they are distributed in a nearly circular pattern. They share the common features of a compact, dusty head (sometimes with a bright rim) and a comet-like tail. The tails of the globules generally point radially outwards from the centre of the Vela OB2 association. The axes of these CGs seem to converge on a very small area around at $l_{\parallel} \sim 261°$ and $b_{\parallel} \sim -5°$ (e.g. Reipurth 1983; Zealey et al. 1983). The source of the CG complex is as yet still unclear. A single source may not be responsible for the formation and the evolution of the Gum Nebula complex. ζ Pup and γ^2 Velorum and the two OB associations are considered as the probable source of the ultraviolet (UV) radiation and photoionization of the nebula in the literature.

There are some uncertainties about the distances of ζ Pup and γ^2 Velorum. The estimated *Hipparcos* distance to the Wolf–Rayet WC8+O spectroscopic binary γ^2 Velorum is 258^{-31}_{+41} pc and to the O4I(n)f star ζ Pup it is 429^{-77}_{+120} pc (van der Hucht et al. 1997). However, Pozzo et al. (2000) argued that the distance to the γ^2 Velorum may be the same as that for the Vela OB2 association. Again, the estimated *Hipparcos* distance to the Vela OB2 association is 410 pc (de Zeeuw et al. 1999), and Woermann et al. (2001) estimated a distance of 500 pc to the expansion centre of the association. In this context, an average distance to the CG system as 450 pc is reasonable as adopted by Sridharan (1992).

There have been several studies on the kinematics of the Gum Nebula region to determine whether the system is expanding or not (e.g. Yamaguchi et al. 1999 and references therein). Most of the studies concluded that the molecular material associated with the Gum Nebula is expanding though the expansion velocities obtained from various studies are different from each other. Zealey et al. (1983) and Sridharan (1992) studied the kinematics of the CGs in details and based on the radial-velocity measurements concluded that the CGs are expanding and obtained the expansion velocity of the system as 5 and 12 km s^{-1}, respectively. Woerman et al. (2001) investigated the kinematics of the neutral material around the Gum Nebula. They concluded that the diffuse molecular clouds (DMCs) and CGs form a single expanding shell centred on $l_{\parallel} = 261°$ and $b_{\parallel} = -2°.5$. According to their model, the shell is asymmetric with the radii of the front and back faces as 130 and 70 pc, respectively. They also obtained the expansion velocities of 14 and 8.5 km s^{-1} for the front and back faces, respectively. They suggested the supernova explosion of the companion of ζ Pup about 1.5 Myr ago as the probable origin of the Gum Nebula and the expanding shell.
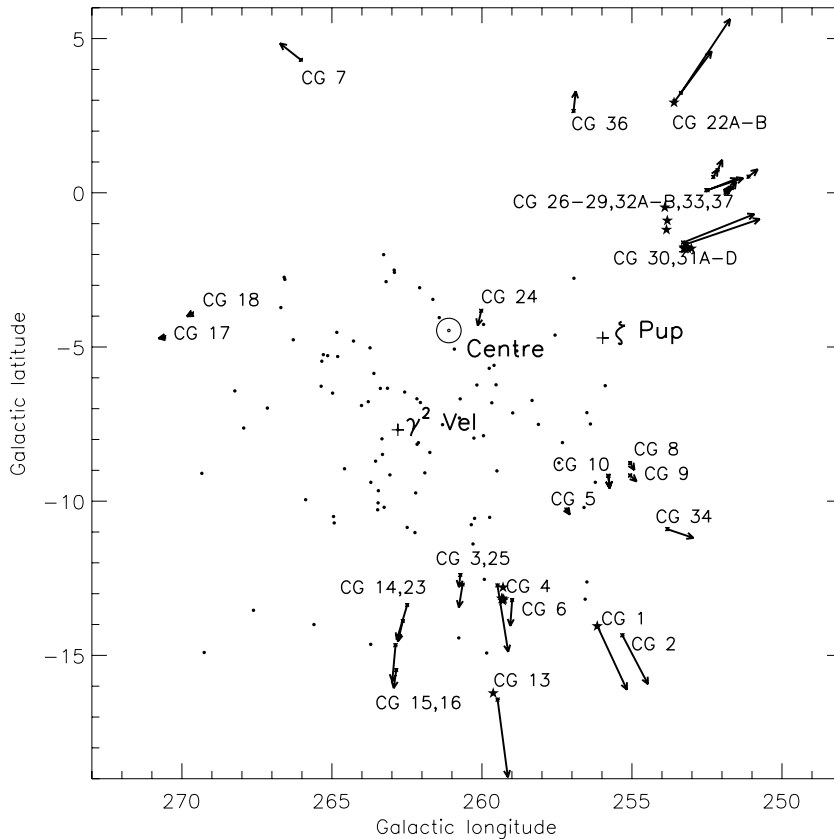
★E-mail: rumpa@iiap.res.in

Figure 1. Distribution of CGs in the Galactic coordinate. The tail vectors have lengths proportional to the tail lengths of the respective CGs. *Filled Circles* represent the members of the Vela OB2 association. *Stars* represent the YSOs around the CGs. Positions of ζ Pup and γ^2 Velorum are also marked.

There have been no studies of the transverse (in the plane of the sky) motion of the Gum Nebula and the associated CGs. In this paper, we have examined the proper motion measurements of stellar and young stellar objects (YSOs) in this region to study the expansion of the system of CGs and possible sources responsible for the triggered star formation in the CGs of the Gum Nebula. In Sections 2 and 3, we summarize the characteristics of the CGs in the Gum Nebula as well as the known YSOs in and around the CGs. We discuss the proper motions of the YSOs in Section 4. Results are discussed in Section 5 and conclusions are presented in Section 6.

2 COMETARY CLOBULES IN THE GUM NEBULA

Zealey et al. (1983) carried out an extensive study of the CGs in the Gum Nebula region. They found 29 CGs within a region of projected angular radius of 9°.5. They tabulated the coordinates, position angles, tail directions and measured H_2CO radial velocities of some of the CGs. They proposed the approximate centre of the CG complex based on the best-fitting circle of the CG positions. Sridharan (1992) found some discrepancies in the coordinates of the CGs and redefined the coordinates of the individual CGs. Sridharan (1992) studied the kinematics of the CGs in the Gum Nebula using the transition lines of ^{12}CO and tabulated the V_{LSR} velocities of most of the CGs. We have adopted the positions and velocities from Sridharan (1992) and the approximate centre of the system from Zealey et al. (1983). Reipurth (1983) suggested that the CGs are pointed towards the triangle formed by ζ Puppis, γ^2 Velorum and Vela Pulsar and estimated an average projected distance of

70 pc for the CGs from the centre of the triangle. It is possible that the two O-type stars and the progenitor of the Vela Pulsar were the main energy source of the whole Gum Nebula region in the past. In Fig. 1, we have plotted the respective CGs, members of the Vela OB2 association and the YSOs around the CGs in the Galactic coordinates together with the probable energy sources γ^2 Velorum and ζ Pup. The adopted centre of the nebula from Zealey et al. (1983) is also plotted. The vectors associated with the CGs in the plot have lengths proportional to the tail lengths of the CGs and also indicate their directions.

Various authors derived the centre of expansion of the CG complex (e.g. Reipurth 1983; Zealey et al. 1983; Sridharan 1992). In this paper, we have adopted the position of the centre as suggested by Zealey et al. (1983) i.e. RA(2000) = $08^h19^m40^s.54$ Dec.(2000) = $-44°09'30''.8$ ($l_{\parallel} \sim 261°.10$, $b_{\parallel} \sim -4°.46$) which is in good agreement with the centre coordinate ($l_{\parallel} \sim 261°.5$, $b_{\parallel} \sim -4°.0$) obtained by Woerman et al. (2001). We have also adopted the approximate centre of the Vela OB2 association as RA(2000) = $08^h07^m00^s.22$ Dec.(2000) = $-46°41'53''.8$ ($l_{\parallel} \sim 262°.3$, $b_{\parallel} \sim -7°.71$).

Reipurth (1983) proposed a mechanism for the formation and evolution of the CGs based on the interaction of the massive stars and their parent molecular cloud. Brand et al. (1983) proposed that the cometary morphology has been created by the passing of shock wave through a spherical molecular cloud. They also suggested the possibility of star formation in the shocked molecular clouds. Analytical models [also known as the radiation driven implosion (RDI) models] have been developed by Bertoldi (1989) and Bertoldi & McKee (1990). Lefloch & Lazareff (1994) studied the evolution and morphology of the CGs by a two-dimensional hydrodynamic

simulation. These models could not reproduce the details of triggered star formation by the UV radiation because they did not include the effect of self gravity. Miao et al. (2006) have shown the evolution of the CGs as well as the triggered star formation under the influence of the UV radiation of the massive stars by a three-dimensional smoothed particle hydrodynamics (SPH) simulation.

According to these models, when an OB association forms in a comparatively dense core of a clumpy giant molecular cloud (GMC), its interaction with its parent molecular cloud can be destructive or constructive depending on the size and density distribution of the leftover clumps and cores of the parent GMC. The UV radiation from the massive young stars evaporates the gas and less dense material in its surroundings and creates an expanding Strömgren sphere. But, it cannot evaporate the relatively dense cores of the clumpy parent cloud because of the recombination shielding of the front layer known as the ionized boundary layer (IBL) (Elmergreen 1976). However, the ionized gas starts to move towards the ionizing source and due to momentum conservation the clumps also get a velocity radially outwards from the central star. This mechanism is known as rocket effect (Oort & Spitzer 1950). The rocket effect pushes the loosely bound gaseous envelope much more effectively than the dense core. The expanding Strömgren sphere also creates a shock wave which interacts with the leftover remnant clumps and converts them into more dense regions. As a result, a newly exposed dense core generally has a thin ionized layer and a tail in the opposite direction created by the leftover material of the parent GMC. At the same time, the compression by the shock front can trigger the next generation star formation in the dense core. It thus provides the additional external pressure force to the gravity to collapse the clumps to form stars. This process of star formation is known as triggered star formation as opposed to the spontaneous star formation where only gravity is responsible for the collapse of the cloud core. Also, the low-mass stars which have formed in these globules simultaneously with the massive stars are exposed to photoevaporation.

Considerable evidence for the current low-mass star formation in the CGs of the Gum Nebula is discussed in the following section.

3 YOUNG STELLAR OBJECTS IN AND AROUND THE COMETRAY GLOBULES

Photometric and spectroscopic studies to investigate the low-mass star formation in the CGs have been undertaken by Petterson (1987), Sahu et al. (1992), Reipurth et al. (1983, 1993) and Kim et al. (2005). Based on Hα emission line, Li absorption line and near-infrared (NIR) excesses, ~30 YSOs have been identified in the direction of the Gum Nebula. There are confirmed signatures of the low-mass star formation in the globules [e.g. CG 1 (Reipurth 1983), CG 22 (Sahu 1992; Reipurth 1983, 1993), CG 30/31/38 complex (Reipurth 1983; Petterson 1987; Kim 2005), CG 4/CG 6/Sa101 and CG 13 (Reipurth 1993)]. We have tabulated the optical and NIR photometric measurements of the individual YSOs in Table 1. We also include the spectral types and the measured Hα equivalent widths in Table 1. NIR magnitudes are taken from the Two-Micron All-Sky Survey (2MASS) Point Source Catalog (Cutri et al. 2003). Except for NX Pup which is of spectral type A, the other YSOs found near the CGs are all late-type stars with spectral types F, K and M. We also tabulate some useful parameters related to the known star-forming CGs and dark clouds in Table 2.

Petterson (1987) made photometric, spectroscopic and infrared (IR) observations of 16 Hα emission-line stars in the region near the CGs: CG 30/31/38. They identified nine T Tauri stars. They also

found that except PHa 12 and PHa 44, all other spectroscopically confirmed YSOs are variable in *V* band. PHa 41 has shown optical variability of ~3 mag, and PHa 15, PHa 21, PHa 34 and PHa 41 have shown large ($U - B$) excesses.

Reipurth & Petterson (1993) surveyed five fields in the Gum Nebula for low-mass emission-line stars. They found seven Hα emission-line stars near the CG4/CG6/Sa 101 cloud complex and one more near CG 13. They confirmed the nature of the objects as the low-mass young stars [RP93] based on the low-resolution spectra, optical and NIR photometry.

Kim, Walter & Wolk (2005) presented photometric and spectroscopic observations of low-mass pre-main-sequence (PMS) stars in the CGs: CG 30/31/38. They identified PMS stars in that direction by the photometric and spectroscopic studies. They confirmed the youth of the PMS stars using the lithium abundances. They also measured the radial velocities of the PMS stars which are consistent with those of the CGs. However, Kim et al. (2005) also suggested that XRS 9, KWW 1055, KWW 1125, KWW 1333 and KWW 1806 are probably the old field stars (50–100 Myr) with strong magnetic activity. We do not consider these objects in further discussion.

There are two YSOs, NX Pup and PHa 92, which are of some special interest. From Figs 4 and 5, it seems very likely that they are embedded in the heads of CG 1 and CG 22, respectively. Both the stars show associated reflection nebulosities, Hα emission line and NIR excess. Based on these observations, Reipurth (1983) concluded that NX Pup is a YSO formed in CG 1. Sahu et al. (1992) also confirmed that PHa 92 is a T Tauri star formed in CG 22. As these two YSOs are still associated with the respective CGs, we can use the proper motion of the two stars as the transverse motion of the respective CGs. The formation and evolutionary models of the CGs predict a net radially outward motion. The CG tails are also directed radially outwards. It should be noted that the tail formation is a relatively fast process and, therefore, the tail direction is determined by the current position of the cloud and the exciting star, while the direction of motion of the star born in the CG would be determined by the initial velocity of the cloud (inertia) and prolonged acceleration, if any, due to the winds, radiation and supernova shocks of massive stars. Here, we have used the proper motion measurements of the YSOs to study the kinematics of the CGs and effects of earlier events in the region on these objects, if any.

4 PROPER MOTION OF THE YOUNG STELLAR OBJECTS

We have collected the available proper motion data on the confirmed YSO candidates from the Naval Observatory Merged Astrometric Dataset (NOMAD) (Zacharias et al. 2005) catalogue. We have selected only those YSOs whose proper motion of at least one component is greater than the error of the measurements given in the catalogue. We have also considered the catalogue by Ducourant et al. (2005) for the proper motion of the PMS stars. The best measurements (smallest error) available in the two catalogues have been selected. However, NOMAD does not have the measurements for NX Pup. We have taken the proper motion measurements for NX Pup from Tycho 2 catalogue (Hog et al. 2000). For the stars taken from NOMAD catalogue, we have converted their proper motion to the galactic coordinates by the formula as described by Mdzinarishvili et al. (2005).

We tabulate the identification number, name, radial distance from the respective star to the NOMAD counterpart (*r*), equatorial coordinates, proper motion measurements and the associated errors in

Table 1. Photometric and spectroscopic measurements of YSOs associated with CGs and DMCs.

Number	Name	V	Spectral type	$W_\lambda(H\alpha)$ A°	J	H	K	Reference[a]
1	NX Pup	10.61[1]	A0[1]	−44.0[5]	8.579 ± 0.030	7.285 ± 0.042	6.080 ± 0.031	1,5
2	KWW 464	15.82	M3V	−2.8	12.126 ± 0.024	11.392 ± 0.026	11.173 ± 0.026	2
3	KWW 1892/PHa 12	15.17	M1V	−26.6/−31.3	11.402 ± 0.023	10.663 ± 0.023	10.323 ± 0.021	2,3
4	KWW 598	17.27	M2V	−11.5	12.150 ± 0.024	11.519 ± 0.023	11.281 ± 0.023	2
5	KWW 1863	14.65	M1V	−2.8	10.873 ± 0.028	10.194 ± 0.033	9.940 ± 0.024	2
6	KWW 1637	12.15	K6V	−2.4	9.529 ± 0.023	8.880 ± 0.022	8.708 ± 0.024	2
7	KWW 873	13.81	K7V	−7.9	10.676 ± 0.023	9.947 ± 0.023	9.578 ± 0.023	2
8	KWW 1043/PHa 15	16.61	M3V	–	11.925 ± 0.028	11.135 ± 0.025	10.628 ± 0.024	2,3
9	KWW 975/Pha 14	15.56	M2V	−8.43	11.387 ± 0.022	10.640 ± 0.025	10.299 ± 0.023	2,3
10	KWW 1302	15.76	M4V	−8.23	11.500 ± 0.032	10.761 ± 0.036	10.429 ± 0.023	2
11	KWW 1953	15.58	M3V	−4.24/−4.93	11.438 ± 0.023	10.722 ± 0.022	10.510 ± 0.023	2
12	KWW 2205	16.20	M4V	−4.34	11.780 ± 0.023	11.122 ± 0.022	10.840 ± 0.021	2
13	KWW XRS 9	–	G5V	3.23	9.783 ± 0.021	9.464 ± 0.022	9.346 ± 0.023	2
14	KWW 1055	14.40	G2V	2.17	12.424 ± 0.026	12.028 ± 0.025	11.890 ± 0.023	2
15	KWW 314	15.14	A3e	6.2	12.546 ± 0.024	12.155 ± 0.023	11.931 ± 0.026	2
16	KWW 1125	12.35	<F8V	5.75	11.285 ± 0.023	11.085 ± 0.023	11.015 ± 0.023	2
17	KWW 1333	13.64	<F8V	5.23	12.074 ± 0.024	11.788 ± 0.027	11.694 ± 0.026	2
18	KWW 1806	13.99	<F8V	0.81	12.262 ± 0.028	11.820 ± 0.031	11.678 ± 0.027	2
19	PHa 44	15.8	K7-M0	−50.7	12.996 ± 0.028	12.175 ± 0.027	11.713 ± 0.019	3
20	PHa 51	15.7	K7-M0	−70.1	12.664 ± 0.027	11.730 ± 0.023	11.090 ± 0.023	3
3	PHa 12	15.5	M1.5	−16.1	11.402 ± 0.023	10.663 ± 0.023	10.323 ± 0.021	3,2
21	PHa 21	16.4	M4	−48.1	12.212 ± 0.026	11.420 ± 0.022	11.058 ± 0.023	3
22	PHa 34	15.6	K3	−60.5	12.439 ± 0.029	11.642 ± 0.026	11.031 ± 0.023	3
23	PHa 40	16.4	M0.5	−18.7	12.750 ± 0.024	11.759 ± 0.022	11.326 ± 0.021	3
24	PHa 41	14.0	–	−98.6	10.775 ± 0.024	9.806 ± 0.022	8.914 ± 0.024	3
8	PHa 15	16.9	M3	−130.5	11.925 ± 0.028	11.135 ± 0.025	10.628 ± 0.024	3,2
9	PHa 14	16.4	M2	−22.0	11.387 ± 0.022	10.640 ± 0.025	10.299 ± 0.023	3,2
25	PHa 92	13.38	K2	−35.4	10.573 ± 0.023	9.692 ± 0.024	9.044 ± 0.021	3
26	[RP93] 1	>17	M3-4	−24.8	11.378 ± 0.023	10.716 ± 0.025	10.406 ± 0.023	4
27	[RP93] 2	>17	M2	−266.5	12.855 ± 0.021	11.932 ± 0.021	11.404 ± 0.020	4
28	[RP93] 3	14.99	K7	−27.0	11.204 ± 0.022	10.218 ± 0.021	9.582 ± 0.020	4
29	[RP93] 4	14.59	K7-M0	−19.3	11.423 ± 0.033	10.669 ± 0.042	10.244 ± 0.031	4
30	[RP93] 5	15.25	K2-5	−126.9	11.959 ± 0.026	10.820 ± 0.030	10.020 ± 0.023	4
31	[RP93] 6	14.21	K7	−5.0	10.445 ± 0.022	9.531 ± 0.022	9.111 ± 0.025	4
32	[RP93] 7	13.97	K5	−9.8	11.491 ± 0.023	10.739 ± 0.023	10.352 ± 0.025	4
33	[RP93] 8	15.33	M1-2	−42.1	11.830 ± 0.027	11.066 ± 0.024	10.832 ± 0.021	4

Notes.[a] (1) Hillenbrand et al. (1992), (2) Kim et al. (2005), (3) Petterson (1987), (4) Reipurth et al. (1993), (5) Manoj et al. (2006).
JHK measurements from the 2MASS ALL-Sky Release Point Source Catalog.

Table 2. Star forming CGs and DMCs.

CGs and the DMCs	l (°)	b (°)	V_{LSR} (km s^{-1})	Vela OB2 Angular separation (°)	Projected distance (pc)	γ^2 Vel Angular separation (°)	Projected distance (pc)	ζ Pup Angular separation (°)	Projected distance (pc)
CG 1	256.14	−14.07	3.3	8.6	67	9.11	71	9.35	73
CG 30/31/38	253.29	−1.61	5.8-7	10.67	84	11.3	89	4.11	32
CG 22	253.58	+2.96	6.5-6.8	13.54	106	14.1	110	7.97	63
CG 13	259.48	−16.43	3.7	9.03	71	9.29	73	12.22	96
CG4/CG6/Sa101	259.48	−12.73	0.9-1.7	5.98	47	6.38	50	9.03	71

Note. V_{LSR} from Sridharan (1992). Projected distances are at 450 pc.

the respective columns of Table 3. The observed differential proper motions of the YSOs with respect to the mean proper motion of the Vela OB2 are tabulated in Columns 10 and 11. The proper motion measurements in galactic coordinates are included in Columns 12 and 13 and the differential proper motion of the YSOs with respect to the mean proper motion of the Vela OB2 in galactic coordinate is tabulated in Columns 14 and 15.

We have tabulated the mean proper motions of the YSOs from Table 3 and the member of the Vela OB2 association (de Zeeuw et al. 1999) from Tycho 2 Catalogue (Hog et al. 2000). From Table 4, it is quite clear that the mean proper motion of all the YSOs is not similar to that of the Vela OB2 members. We consider YSOs 2, 4, 11 and 29 as *high-velocity YSOs* due to their proper motions being greater than 2σ from the mean in both the components. We

Table 3. Proper Motion of the YSOs associated with CGs and DMCs.

Number	Name	r (arcsec)	RA (2000)	Dec. (2000)	$\mu_\alpha \cos\delta$ (mas yr^{-1})	e (mas yr^{-1})	μ_δ (mas yr^{-1})	e (mas yr^{-1})	$\Delta\mu_\alpha \cos\delta$ (mas yr^{-1})	$\Delta\mu_\delta$ (mas yr^{-1})	$\mu_l \cos b$ (mas yr^{-1})	μ_b (mas yr^{-1})	$\Delta\mu_l \cos b$ (mas yr^{-1})	$\Delta\mu_b$ (mas yr^{-1})
1	NX Pup	0.123	071 928.26	−443 511.4	−4.2	2.0	6.1	1.9	2.22	−2.03	−7.08	−1.26	3.32	0.04
3	KWW 1892	0.101	080 822.15	−360 347.0	−6.5	4.8	7.7	4.7	−0.08	−0.43	−9.99	−1.29	0.41	0.01
6	KWW 1637	0.259	080 839.27	−360 501.7	−7.7	2.8	8.6	2.7	−1.28	0.47	−11.40	−1.81	1.00	−0.51
7	KWW 873	0.024	080 845.40	−360 840.2	−8.4	4.7	4.6	4.7	−1.98	−3.53	−8.42	−4.56	1.98	−3.26
8	KWW 1043	0.354	080 846.82	−360 752.8	−7.0	4.8	8.5	4.8	−0.58	0.37	−10.94	−1.27	0.54	0.03
9	KWW 975	0.099	08 08 33.87	−360 809.8	−5.9	4.8	12.3	4.8	0.52	4.17	−13.53	1.71	3.13	3.01
20	PHa 51	0.069	081 247.04	−361 917.9	−6.4	4.6	0.5	4.6	0.02	−7.63	−3.98	−5.03	2.59	−0.37
22	PHa 34	0.061	081 356.07	−360 802.1	−5.7	4.7	5.6	4.7	0.72	−2.53	−7.81	−1.67	4.06	−3.37
24	PHa 41	0.014	081 555.32	−355 758.1	−7.4	4.6	2.7	4.6	−0.98	−5.43	−6.34	−4.67	6.42	−3.73
25	PHa 92	0.041	082 840.70	−334 622.3	−6.6	4.6	10.4	4.6	−0.18	2.27	−12.30	0.71	1.90	2.01
28	[RP93] 3	0.987	073 110.81	−470 032.5	−6.7	5.0	10.9	4.9	−0.28	2.77	−12.73	−1.29	2.33	0.01
30	[RP93] 5	1.104	073 136.68	−470 013.2	−6.9	5.0	8.4	5.0	−0.48	0.27	−10.57	−2.54	0.17	−1.24
31	[RP93] 6	0.541	073 137.42	−470 021.5	−7.0	4.9	3.6	5.0	−0.58	−4.53	−6.29	−4.73	4.11	−3.43
32	[RP93] 7	1.501	073 326.86	−464 842.6	−3.2	4.9	11.1	4.9	3.22	2.97	−11.37	2.03	0.97	3.33
33	[RP93] 8	0.363	071 540.89	−483 127.3	−4.5	5.8	7.1	5.9	1.92	−1.03	−8.29	−1.39	2.11	−0.09
2	**KWW 464**	0.404	080 800.66	−355 733.3	−17.4	4.7	17.5	4.7	−10.98	9.37	−24.13	−5.17	−13.73	−3.87
4	**KWW 598**	1.089	080 837.60	−360 949.4	−10.0	18.0	24.0	5.0	−3.58	15.87	−25.59	4.61	−15.19	5.91
11	**KWW 1953**	0.103	080 826.93	−360 335.4	−13.0	4.9	13.1	5.0	−6.58	4.97	−18.05	−3.83	−7.65	−2.53
29	**[RP93] 4**	1.177	073 121.85	−465 743.9	−24.9	4.9	32.0	4.9	−18.48	23.87	−39.66	−8.47	−29.26	−7.17

Note. Differential proper motions are given with respect to Vela OB2 association. The *high-veocity YSOs* (2, 4, 11, 29) have been highlighted in bold.

Table 4. Statistics of proper motion of the YSOs and Vela OB2 members.

Objects	$\langle \mu_\alpha \cos\delta \rangle$ (mas yr^{-1})	$\sigma(\mu_\alpha \cos\delta)$ (mas yr^{-1})	$\langle \mu_\delta \rangle$ (mas yr^{-1})	$\sigma(\mu_\delta)$ (mas yr^{-1})
All YSOs	-8.39	5.12	10.25	7.53
High-velocity YSOs	-16.33	6.47	21.65	8.23
Normal-velocity YSOs	-6.27	1.38	7.20	3.37
Vela OB2 members	-6.42	2.45	8.13	1.93

discuss the properties of *high-velocity YSOs* in detail in Section 5. Excluding the *high-veocity YSOs*, the rest of the YSOs are termed as *normal-velocity YSOs*. The mean proper motion of the *normal-velocity YSOs* is similar to the mean motion of the members of the Vela OB2 association within the error limit associated with the measurements of the proper motion. We have plotted the histogram of the proper motion of both the *normal-velocity YSOs* and *high-veocity YSOs* with the Vela OB2 association in Fig. 2.

The heliocentric velocity of the association $V_{helio} = 18$ km s^{-1} (de Zeeuw et al. 1999), which is equivalent to $V_{LSR} = 4$ km s^{-1}. The radial velocities of the CGs and DMCs are taken from Sridharan (1992), Woermann et al. (2001) and Otrupcek, Hartley & Wang (2000), respectively. The mean $V_{LSR}(\langle V_{LSR}\rangle)$ of the CGs is 1.74 km s^{-1} with $\sigma_{V_{LSR}} = 4.73$. Among all the CGs, only CG 24 has radial velocity more than 2σ away from the mean. Excluding CG 24, $\langle V_{LSR}\rangle$ for rest of the CGs is 2.13 with $\sigma_{V_{LSR}} = 4.13$. $\langle V_{LSR}\rangle$ of the DMCs is 5 km s^{-1} with $\sigma_{V_{LSR}} = 6$ km s^{-1}. Out of the 106, 96 DMCs have values within 2σ of the calculated mean. $\langle V_{LSR}\rangle$ of these 96 DMCs is 3.5 km s^{-1} with $\sigma_{V_{LSR}} = 4.52$ km s^{-1}. These values indicate that there is a good coupling between the CGs, DMCs and the members of the Vela OB2 associations. All these systems of objects have the same average motion.

5 DISCUSSION

Woermann et al. (2001) have suggested that the supernova explosion of the massive binary companion of the ζ Pup is responsible for the origin of the Gum Nebula. They estimated that the explosion took place $\sim$1.5 Myr ago. They also suggested that the runaway O star ζ Pup was within <0.5 of the expansion centre of the neutral shell $\sim$1.5 Myr ago. As a first-order estimate, we have traced back the proper motion of ζ Pup and Pha 92 and NX Pup (embedded YSOs) in Galactic coordinates, and calculated their angular separations. The angular separation of PHa 92 and NX Pup from ζ Pup as a function of time in the past is plotted in Fig. 3. We do not see any indication of convergence between all three in the last 1.5 Myr. This trend suggests that the supernova explosion of the companion of the ζ Pup did not give any radial motion to the stars NX Pup and PHa 92. So, the supernova explosion was not responsible for the bulk motion of CG 1 and CG 22 associated with NX Pup and PHa 92, respectively.

Woermann et al. (2001) also gave a likely configuration of the Gum nebula. They suggested that most of the CGs and the Vela OB2 association is situated within the front face of the expanding shell. The expected transverse velocity components of the two stars based on the radial velocities of the CGs and the expansion velocity
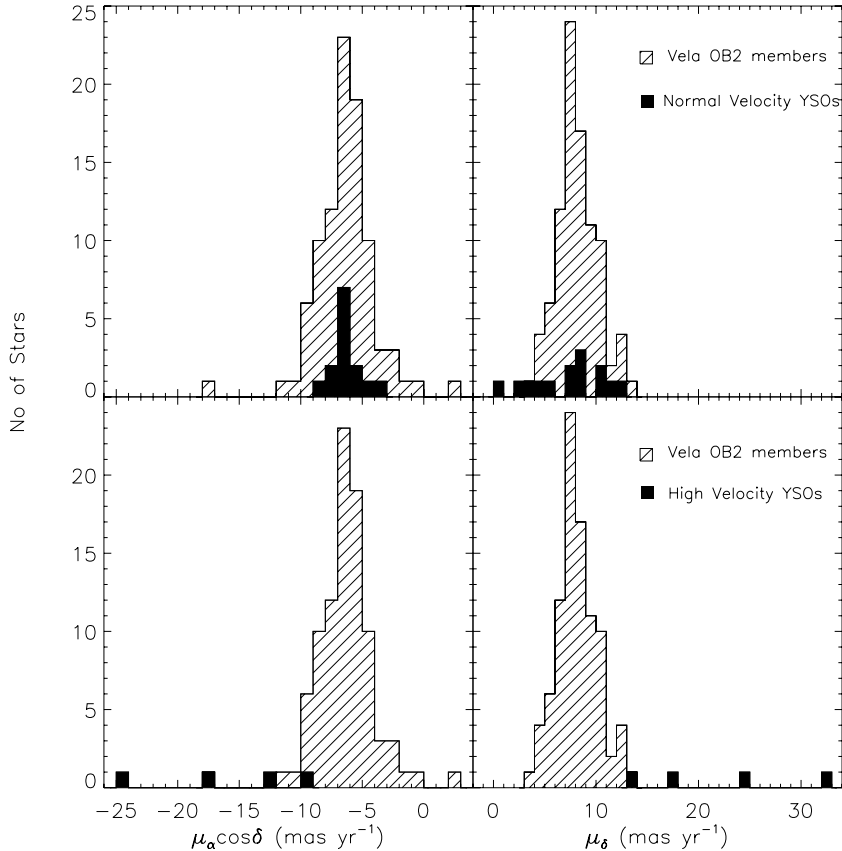

Figure 2. Proper motion histograms of *normal-velocity YSOs*, *high-veocity YSOs* and the members of Vela OB2 association. *Line-filled* histogram represent the members of the association and the *solid* histogram represent the YSOs.
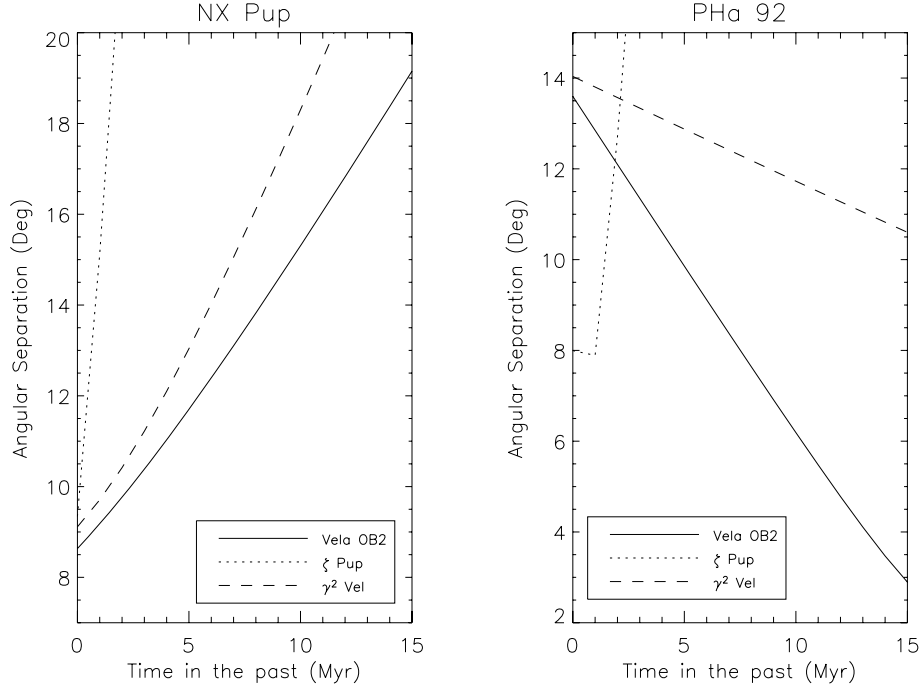
Figure 3. Angular separation of NX Pup and PHa 92 from ζ Pup, γ^2 Vel and Vela OB2 association in the past. The *dotted*, *dashed* and *solid* lines represent the angular separation from ζ Pup, γ^2 Vel and Vela OB2 association, respectively.

of the system can be calculated using the following formula: $V_T = \sqrt{V_{\exp}^2 - V_{\mathrm{radial}}^2}$.

Considering V_{LSR} (CG 1) = +3.3 km s^{-1} and V_{LSR} (CG 22) = 6.65 km s^{-1} from Sridharan (1992) and $V_{\exp}$ = 14 km s^{-1} for the front face from Woermann et al. (2001), we obtained the expected transverse velocity components as V_T (CG 1) = 13.6 km s^{-1} and V_T (CG 22)= 12.32 km s^{-1}. These values correspond to 5.78 and 6.38 mas yr^{-1} for CG 1 and CG 22, respectively, with respect to the centre of explosion. Again, if CG 22 and CG 1 were close to the site of supernova explosion of the companion of ζ Pup 1.5 Myr ago, then the proper motions of NX Pup and Pha 92 born in the respective CGs should be consistent with their motion from the site of the explosion to their present position. This would require a differential proper motion of NX Pup as $\Delta\mu_l \cos b \sim -30.09$ mas yr^{-1}, $\Delta\mu_b \sim -36.23$ mas yr^{-1} and PHa 92 as $\Delta\mu_l \cos b \sim -39.73$ mas yr^{-1}, $\Delta\mu_b \sim 1.01$ mas yr^{-1}. At present, we do not have the proper motion of the binary companion of ζ Pup which is the suggested centre of the expansion. But the other O-type star γ^2 Vel shares a similar kind of motion as Vela OB2. So, it is reasonable to adopt the mean proper motion of Vela OB2 for the motion of the centre. Considering the mean proper motion of the Vela OB2, the expected proper motion of NX Pup is $\mu_l \cos b \sim -40.49$ mas yr^{-1}, $\mu_b \sim -41.03$ mas yr^{-1} and for PHa 92 it is $\mu_l \cos b \sim -50.13$ mas yr^{-1}, $\mu_b \sim 2.31$ mas yr^{-1}.

Considering the earliest stars, Yamaguchi et al. (1999) suggested the age of the association as less than 10 Myr. We also traced back the proper motion of Pha 92 and NX Pup from the γ^2 Velorum and the mean proper motion of the Vela OB2 association up to 15 Myr. Fig. 3 also shows the angular separations of NX Pup and PHa 92 from γ^2 Vel and Vela OB2 association. There is no indication of the convergence of NX Pup with any of the sources (ζ Pup, γ^2 Velorum and Vela OB2) plotted in the diagram. However, the angular separation between the PHa 92 and

the Vela OB2 association was shorter in the past than the present separation.

Adopting the proper motion of Vela OB2 for the motion of the centre, the observed differential proper motion of the stars with respect to the Vela OB2 association is estimated and tabulated in Table 3 (Column 15 and 16). There is a significant mismatch between the expected and observed differential proper motions of the YSOs with respect to the Vela OB association. For NX Pup, the expected differential proper motion is $\Delta\mu_l \cos b \sim -30.09$ mas yr^{-1}, $\Delta\mu_b \sim -36.23$ mas yr^{-1}, while the observed differential proper motion is $\Delta\mu_l \cos b \sim 3.32$ mas yr^{-1}, $\Delta\mu_b \sim 0.04$ mas yr^{-1}. For PHa 92, the expected differential proper motion is $\Delta\mu_l \cos b \sim -39.73$ mas yr^{-1}, $\Delta\mu_b \sim 1.01$ mas yr^{-1} while the observed differential proper motion is $\Delta\mu_l \cos b \sim 1.90$ mas yr^{-1}, $\Delta\mu_b \sim 2.01$ mas yr^{-1}. For other YSOs, the expected differential proper motion is $|\Delta\mu| \sim 30$ mas yr^{-1} while the observed differential proper motion is $|\Delta\mu| \sim 5$ mas yr^{-1}.

The proper motion vector **P**1 of NX Pup (star identification No 1 in Table 1) is plotted on the Digitized Sky Survey (DSS) image of CG 1 in Fig. 4. The differential proper motion vector **D**1 of NX Pup with respect to Vela OB2 association is also plotted in Fig. 4. The proper motion vector **P**25 of PHa 92 (Star identification No 25 in Table 1) is plotted on the DSS image of CG 22 in Fig. 5. The differential proper motion vector **D**25 of PHa 92 with respect to the Vela OB2 association is also plotted in Fig. 5. The directions towards the Vela OB2 association and ζ Pup are also shown in Figs 4 and 5. Within the errors associated with the proper motion measurements, we do not find any clear evidence for the transverse motion for these two stars away from the site of supernova explosion of the companion of ζ Pup. For the objects which are not embedded in any CGs but supposed to be associated with the Gum Nebula, we get similar results. They also do not show any indication of expansion within the errors of proper motion measurements. This suggests that
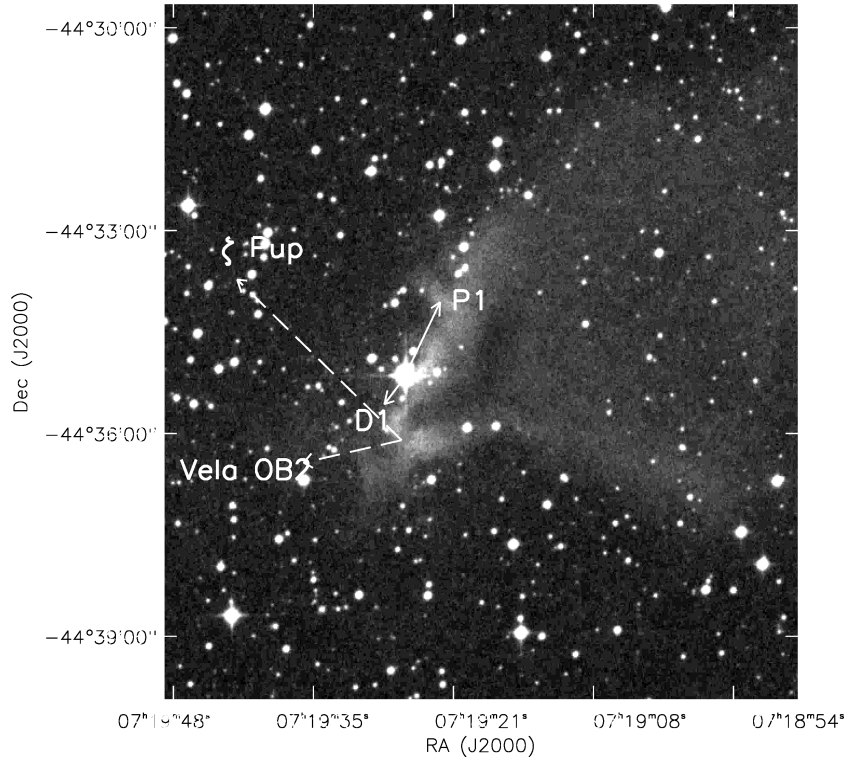
Figure 4. Proper motion vector *P*1 of NX Pup plotted on the DSS image of CG 1. The directions towards the Vela OB2 association and ζ Pup are also shown by *dashed* lines. The differential proper motion vector *D*1 is also plotted. Arrow lengths are proportional to the respective proper motion.
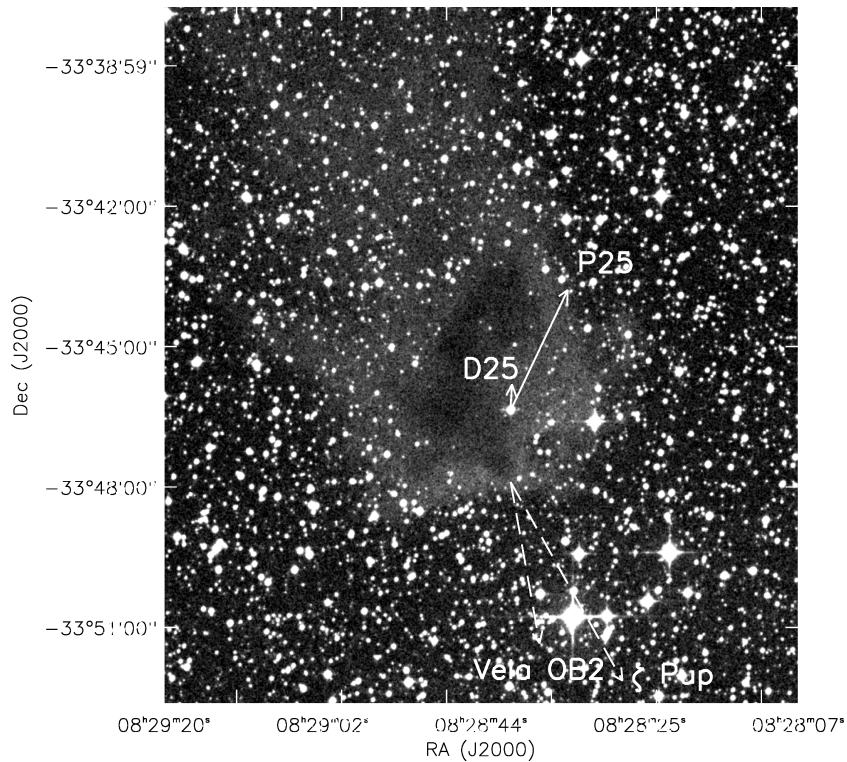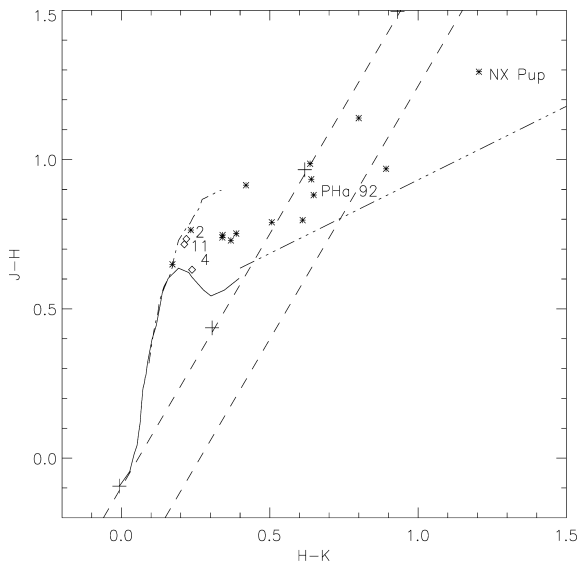

Figure 5. Proper motion vector *P*25 of PHa 92 plotted on the DSS image of CG 22. The directions towards the Vela OB2 association and ζ Pup are also shown by *dashed* lines. The differential proper motion vector *D*25 is also plotted. Arrow lengths are proportional to the respective proper motion.

Figure 6. 2MASS JHK colour–colour diagram for the known YSOs in and around the CGs with reliable NIR photometry. High-veocity stars are marked with *diamond* and their corresponding number from Table 1. *Solid* and *dash–dotted* curves are the locations of main-sequence and giant stars from Bessell & Brett (1988) converted into 2MASS as suggested by Carpenter (2001). The two *dashed* parallel lines, with the slope derived from interstellar reddening law (Rieke & Lebofsky 1985), separate CTTSs from Herbig Ae/Be and from reddened main-sequence stars (Lee et al. 2000). The *dash–dotted* line is the dereddened CTTS locus (Meyer et al. 1997). Points marked with *plus* on the dashed line are at an interval of $A_v = 5$ mag.

the system of CGs share the mean motion of Vela OB2 and do not show any systematic radial motions away from the centre.

We have also found three high-velocity YSOs in CG 30 complex and one more in Sa 101. They have proper motion measurements more than 3σ away from the mean proper motion of the Vela OB2. For the stars in the CG 30 complex, Kim et al. (2005) have estimated an age of 2–5 Myr. These YSOs have Hα emission line as well as Li absorption line indicating *youth*. Fig. 6 gives a NIR $J - H$ versus $H - K$ colour–colour (CC) diagram of the known YSOs in and around the CGs with reliable NIR photometry as given in Table 1. high-veocity stars are marked with *diamond* and their corresponding identification number, as given in Table 1. We exclude the high-veocity star [RP93] 4 from the CC diagram due to poor measurements. The location of normal main-sequence and giant stars from Bessell & Brett (1988) is modified to the 2MASS photometry as suggested by Carpenter (2001) and plotted with *solid* and *dash–dotted* lines, respectively. Points marked with *plus* on the dashed line are at an interval of $A_v = 5$ mag. Lee et al. (2005) have developed an empirical and effective set of criteria, based on the 2MASS colours, to select candidate classical T Tauri stars (CTTSs). They found that the CTTS lies approximately between the two parallel *dashed* lines, defined empirically by $(j\_m - h\_m) - 1.7(h\_m - k\_m) + 0.0976 = 0$ and $(j\_m - h\_m) - 1.7(h\_m - k\_m) + 0.450 = 0$, where j_m, h_m and k_m are 2MASS magnitudes, and the slope is specified by the interstellar reddening law (Rieke & Lebofsky 1985). The *dash–dotted* line in the CC diagram represents the dereddened CTTS locus (Meyer et al. 1997), modified to the 2MASS photometry (Carpenter 2001) with $(j\_m - h\_m) - 0.493(h\_m - k\_m) - 0.439 = 0$. The *dashed* parallel lines separate CTTS from Herbig Ae/Be and from reddened main-sequence stars. Positions occupied by the objects in the CC diagram give primary information about the

nature of the YSOs. NX Pup (Herbig Ae) and PHa 92 (T Tauri) both have NIR excesses and their positions in the CC diagram also match with the criteria suggested by Lee et al. (2005). It is interesting to note that most of the YSOs which have similar proper motion as Vela OB2, show NIR excesses but all the three high-veocity YSOs occupy similar positions in the CC diagram and they do not show NIR excesses. But there are no significant differences in Hα or Li equivalent widths and radial velocities of these objects as compared with the other stars and the CGs (Kim et al. 2005). If they are indeed associated with the CG 30 complex then they perhaps owe their high velocities to the process of star formation in the cloud which is not understood. It may also be possible that the cause of their high proper motion affected their circumstellar environment and as a result they do not have IR excesses. There have been suggestions that during the star formation in binary or multiple systems YSOs can gain high velocities due to dynamical interactions (Sterzik et al. 1995; Gorti & Bhatt 1996, Reipurth 2000). But CG 30 lies close to Galactic plane. So it is also possible, but unlikely, that these objects are foreground YSOs moving with relatively higher velocities and large proper motions.

6 CONCLUSION

In the analysis presented above, no clear evidence is found for the supernova explosion of the binary companion of ζ Pup causing expansion of the system of CGs in the Gum Nebula. We also do not find any systematic transverse expansion of the YSOs and the CGs in the Gum Nebula. It is possible that the CGs retain the initial velocities of their parent clumps inside the GMC characterized by a velocity dispersion as seen in the radial velocities. The energy sources in the Gum Nebula (stellar wind, radiation and supernova explosions) perhaps sweep out the diffuse material but not the relatively dense and massive CGs. The absence of CGs within some radius ($\sim 9°$) of the OB association would then require destruction due to evaporation by the UV radiation (Reipurth 1983) from the central energy sources. No clear evidence is found for transverse motion of YSOs and CGs as predicted by RDI models.

REFERENCES

Bertoldi F. M., 1989, ApJ, 346, 735
Bertoldi F. M., McKee C., 1990, ApJ, 354, 529
Bessell M. S., Brett J. M., 1988, PASP, 100, 1134

Brand P. W. J. L., Hawarden T. G., Longmore A. J., Williams P. M., Caldwell J. A. R., 1983, MNRAS, 203, 215

Carpenter J. M., 2001, AJ, 121, 2851

Chanot A., Sivan J. P., 1983, A&A, 121, 19

Cutri R. M. et al., 2003, (NASA/IPAC Infrared Science Archive, The IRSA 2MASS All-Sky Point Source Catalog)

de Zeeuw P. T., Hoogerwerf R., de Bruijne J. H. J., Brown A. G. A., Blaauw A., 1999, AJ, 117, 354

Ducourant C., Teixeira R., Perie J. P., Lecampion J. F., Guibert J., Sartori M. J., 2005, A&A, 438, 769

Elmergreen B. G., 1976, ApJ, 205, 405

Gorti U., Bhatt H. C., 1996, MNRAS, 278, 611

Gum C. S., 1952, Observatory, 72, 151

Hillenbrand L. A., Strom S. E., Vrba F. J., Keene J., 1992, ApJ, 397, 613

Hog E. et al., 2000, A&A, 355, L27

Kim J. S., Walter F M., Wolk S. J., 2005, AJ, 129, 1564

Lee H.-T., Chen W. P., Zhang Z.-W., Hu J.-Y., 2005, ApJ, 624, L808

Lefloch B., Lazareff B., 1994, A&A, 289, 559

Manoj P., Bhatt H. C., Maheswar G., Muneer S., 2006, ApJ, 653, 657

Mdzinarishvili T. G., Chargeishvili K. B., 2005, A&A, 431, L1

Miao J., White G. J., Nelson R., Thompson M., Morgan L., 2006, MNRAS, 369, 143

Oort J. H., Sitzer L. Jr., 1955, ApJ, 121, 6

Otrupcek R. E., Hartley M., Wang J.-S., 2000, PASA, 17, 92

Petterson B., 1987, A&A, 171, 101

Pozzo M., Jeffries R. D., Naylor T., Totten E. J., Harmer S., Kenyon M., 2000, MNRAS, 313, L23

Reipurth B., 1983, A&A, 117, 183

Reipurth B., 2000, AJ, 120, 3177

Reipurth B., Petterson B., 1993, A&A, 267, 439

Rieke G. H., Lebofsky M. J., 1985, ApJ, 288, 618

Sahu M., Sahu K. C., 1992, A&A, 259, 265

Sridharan T. K., 1992, A&A, 13, 217

Sterzik M. F., Durisen R. H., 1995, A&A, 304, L9

van der Hucht et al., 1997, New Astron., 2, 245

Woermann B., Gayland M. J., Otrupeck R., 2001, MNRAS, 325, 1213

Yamaguchi N., Mizuno N., Moriguchi Y., Yonekura Y., Mizuno A., Fukui Y., 1999, PASJ, 51, 765

Zacharias N., Monet D., Levine S., Urban S., Gaume R., Wycoff G., 2004, BAAS, 36, 1418

Zealey W. J., Ninkov Z., Rice E., Hartley M., Tritton S. B., 1983, Astrophys. Lett., 23, L119

This paper has been typeset from a TEX/LATEX file prepared by the author.